TURBULENT BOUNDARY LAYER STRUCTURE OVER SPARSELY-DISTRIBUTED ROUGHNESS

B. Ganapathisubramani
School of Engineering Sciences,
University of Southampton
Highfield, Southampton, SO17 1BJ, UK
g.bharath@soton.ac.uk

M. P. Schultz
Department of Naval Architecture & Ocean Engineering,
US Naval Academy,
Annapolis, MD 21402, USA
mschultz@usna.edu

ABSTRACT

Experiments were performed on a surface consisting of sparsely-distributed rigid circular cylinder roughness elements to examine the effects of sparseness on turbulence structure. Measurements were made using both two-component LDV and wide-field planar PIV techniques. The mean velocity profile in defect form conforms to outer-layer similarity. The streamwise and wall-normal turbulence intensities appear to exhibit outer-layer similarity for $y > 3k_s$. However, the Reynolds shear stress is consistently higher compared to smooth-wall as well as other rough-wall data. The higher shear stress appear to be linked with strong ejection events that characterise the outer region of the flow. Two-point spatial correlations of both streamwise and wall-normal velocity fluctuations indicate that the turbulent structures in the outer region are coherent over much larger streamwise distances compared to smooth and other rough-wall cases. These results point to the fact that sparseness plays an important role in the outer-layer structure of turbulent boundary layers over rough walls.

INTRODUCTION

The importance of surface roughness in boundary-layer flows is well known. The roughness elements promote transition to turbulence and the pressure forces acting on these elements increase the drag. Prediction of these roughness effects is of clear importance in a variety practical applications. In most cases, this prediction is achieved through turbulence modelling, which in turn, requires prediction of the Reynolds stresses. The behaviour of these Reynolds stresses depends on the structure of the boundary layer, and therefore, it is important to develop a fundamental understanding of the structure of boundary layers over different surface conditions. It could also be noted that roughness allows the fundamental interactions between the inner and outer layer to be probed (i.e. is the classical 'bottom up' model or the more recent 'top down' concept of the TBL more accurate?).

A variety of previous studies have examined the effect of roughness on the structure of turbulence. Raupach, Antonia & Rajagopalan (1991) performed an extensive literature review and found strong evidence for outer-layer similarity in the structure of turbulence in both rough and smooth walls. This outer-layer similarity, often referred to as Townsend's similarity hypothesis, states that at high Reynolds number, turbulent motions are independent of wall roughness, i.e., the topology and form of the wall does not impact the structure of turbulence. However, it must be noted that most previous studies were performed over three-dimensional rough surfaces. Experimental studies of rough-wall boundary layers by Krogstad & Antonia (1999) and subsequently by Volino, Schultz & Flack (2009) have indicated significant changes to the Reynolds stresses that extend well into the outer layer for flows over two-dimensional roughness. Jimenez (2004) suggested that the agreement/violation of the similarity hypothesis may be an effect of the relative roughness height, k/δ (where k is the roughness height and δ is the boundary layer thickness), on the flow. He observed that the roughness height is large compared to the boundary-layer thickness ($k/\delta > 1/50$) in cases where the outer-layer similarity is violated. However, Flack, Schultz & Connelly (2007) showed the presence of outer-layer similarity for flows over for sand-grain and mesh surfaces that had a $k/\delta \approx 1/20$. Recent results by Amir & Castro (2011) suggest that the similarity extends to even larger relative roughness (k/δ up to 0.15). This suggests that additional effects might be responsible for the break-down of outer-layer similarity.

One possible source that might affect the turbulent flow structure is the surface density of the roughness. This surface density, also known as solidity (λ_f) is a characteristic parameter of a rough surface and is defined as the total projected frontal roughness area per unit wall-parallel projected

area. Schlichting (1936) performed a wide range of experiments and found that there are two regimes of solidity: dense & sparse. In the dense regime ($\lambda_f > 0.15$), the roughness effect, which can be detected by the downward shift in the logarithmic law of the wall, decreases with increased solidity because the roughness elements shelter each other. However, in the sparse regime ($\lambda_f < 0.15$), the effect of the roughness increases with increasing solidity. Interestingly, the 2-D bars of Volino *et al.* (2009) ($\lambda_f \approx 0.15$), is at the interface of sparse and dense regimes. It is unclear if the breakdown of outer-layer similarity in flow over these bars is an effect of their geometry or surface density. Therefore, it is essential to isolate the effects of geometry from surface density of roughness. However, almost all previous studies in the literature that explored the structure of rough-wall boundary-layers have focussed on rough-surfaces with high solidity (i.e. dense regime), where roughness elements shelter each other. Very little information is available on the structure of boundary-layer flows over sparse-roughness. Therefore, in this study we explore the structure of rough-wall boundary-layer flow over a surface with sparsely distributed 3-D roughness elements.

EXPERIMENTAL FACILITY AND DETAILS

Experiments were conducted in a water tunnel designed for detailed boundary-layer measurements. The test section was 2m long, 0.2m wide and nominally 0.1m high. The lower wall was a flat plate which served as the test wall. The upper wall was adjustable and set for a zero streamwise pressure gradient. The upper wall and sidewalls provided optical access.

The rough-surface consisted of spanwise rows of 4 mm tall stainless steel cylindrical elements (nominal diameter 1 mm). The cylinders are lined up in spanwise rows (with spanwise spacing of 10 mm) and are staggered in the streamwise direction (streamwise spacing between nearest elements is 10 mm) with each element positioned centrally between the two nearest upstream elements. This resulted in the elements in subsequent rows being offset in the spanwise direction by 5 mm, which in turn minimises the sheltering effect and increases λ_f. Based on this configuration, the solidity of the surface was 0.08, which is in the sparse regime. Measurements were carried out at two different flow conditions, and the details are given in table 1.

Boundary-layer velocity measurements were obtained with a TSI FSA3500 two-component laser-Doppler velocimeter (LDV). The LDV consists of a four-beam fibre optic probe that collects data in backscatter mode. A custom-designed beam displacer was added to the probe to shift one of the four beams, resulting in three co-planar beams that can be aligned parallel to the wall. Additionally, a 2.6:1 beam expander was located at the exit of the probe to reduce the size of the measurement volume. The resulting probe volume diameter (d) was 45μm with a probe volume length (l) of 340μm.

Flow-field measurements were acquired using particle image velocimetry (PIV). Streamwise–wall normal (x, y) planes were acquired at the spanwise centreline of the test section. The flow was seeded with 2μm silver coated glass spheres. The seed particles were illuminated by pulsed laser sheets (thickness $\approx$ 1 mm) from a pair of flashlamp pumped

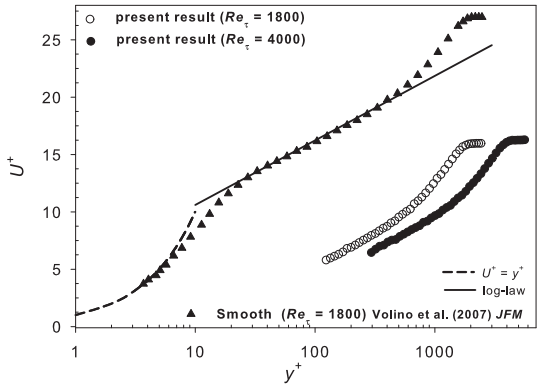

Figure 1. Mean velocity profiles normalised by inner scales. Smooth-wall data at $Re_\tau = 1800$ are shown for comparison (from Volino *et al.* (2007)).

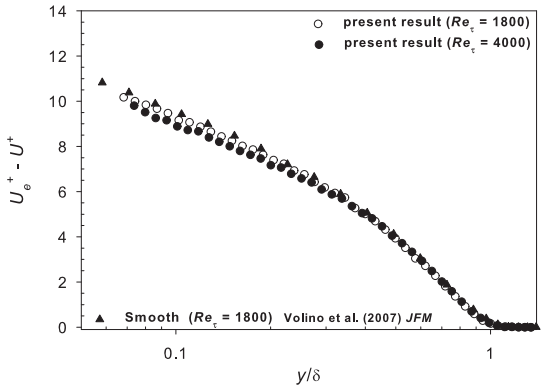

Figure 2. Mean velocity profiles in defect form normalised by outer scales. Smooth-wall data at $Re_\tau = 1800$ are shown for comparison (from Volino *et al.* (2007)).

Nd:YAG lasers directed through the top of the tunnel. Sets of digital images were captured by two *TSI Powerview* CCD cameras ($2k \times 2k$ pixels) lined up next to each other in the streamwise direction to provide a wide field of view whose area was approximately 210×105mm^2. Nikon Nikkor 50 mm f/1.2 lenses were used with both cameras. Velocity vectors were obtained using 32 pixel square windows with 50% overlap using the *TSI Insight 3G* software. For each test case, 1000 image pairs were acquired with each camera for processing.

Results

Point measurements

Mean velocity profiles in law-of-the-wall form and defect form at two different Reynolds numbers are shown in figures 1 and 2, respectively. Data from a smooth-wall boundary layer at a comparable Reynolds number are also shown. As expected, figure 1 shows that the downward shift in the mean profiles increases with increasing Reynolds number.

Wall	Symbol	U_e (m/s)	U_τ (m/s)	δ (mm)	Re_τ	k_s^+	k/δ	ΔU^+
Sparse Cylinders (low Re)	○	0.603	0.0378	44.0	1813	381	0.091	11.0
Sparse Cylinders (high Re)	●	1.422	0.0875	42.1	4000	662	0.095	12.3
Smooth Wall (Volino *et al.* 2007)	▲	1.255	0.0465	35.2	1772	–	–	–

Table 1. Boundary-layer parameters.

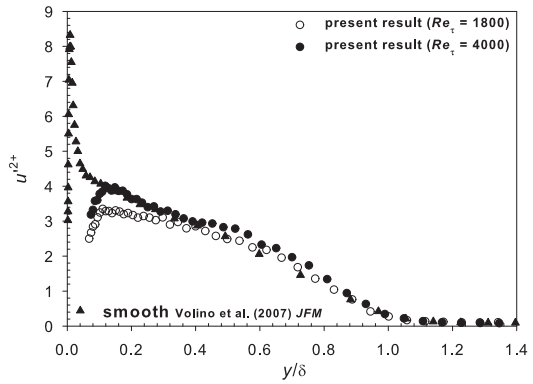

Figure 3. Wall-normal variation of streamwise turbulence intensity ($\overline{u'^2}/U_\tau^2$).

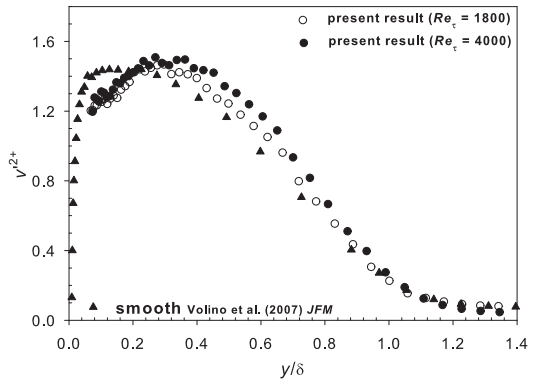

Figure 4. Wall-normal variation of wall-normal turbulence intensity ($\overline{v'^2}/U_\tau^2$).

The roughness function (ΔU^+), which captures this downward shift in the log region, for both Reynolds numbers is listed in table 1. Figure 2 indicates no visible differences in defect profiles in the outer region. These results indicate that the mean flow in the outer layer is fairly insensitive to surface conditions.

Figures 3 and 4 show the streamwise and wall-normal turbulent intensities in outer coordinates and are compared to the smooth-wall results. Figure 1 indicates that all three profiles collapse in the outer region (i.e. for $y/\delta > 0.4$). The smooth-wall data show the near-wall peak, however, this is diminished in the rough-wall data due to the presence of roughness elements. The streamwise intensity over the rough-wall at $Re_\tau = 4000$ is higher than that at $Re_\tau = 1800$ indicating a Reynolds number effect in the near-wall region. Figure 4 shows that the wall-normal intensity for the rough-wall case is consistently higher (albeit only marginally) in the outer region. The difference between the smooth-wall case and the rough-wall case in the outer region ($0.2 < y/\delta < 0.8$) at the same Reynolds number is approximately 10% (which is higher than the measurement uncertainty). This suggests that the presence of the roughness elements affects the structure of boundary layers in the outer region. Moreover, the higher Reynolds number case exhibits a higher turbulence intensity compared to the lower Reynolds number case in the outer region.

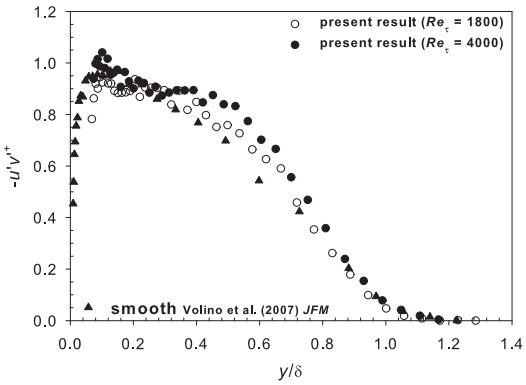

Figure 5. Wall-normal variation of Reynolds shear stress ($\overline{-u'v'}/U_\tau^2$).

Figure 5 shows the wall-normal profiles of Reynolds shear stress for the rough-wall (at both Reynolds numbers) and the smooth-wall. The wall-normal behaviour of Reynolds shear stress appears to be similar to that of wall-normal turbulence intensity in figure 4 with difference in the profiles noted in outer region ($0.2 < y/\delta < 0.8$). The higher Reynolds number data exhibits a plateau region in the outer region which is absent in the other two cases.

In order to further understand the Reynolds shear stress behaviour, a quadrant analysis(Wallace, Eckelmann & Brodkey 1972) is carried out. This analysis sorts turbulent events into each of the four quadrants of the $u' - v'$ plane thereby allowing us to understand the events that lead to mean momentum transfer. In particular, it allows the contributions of ejection ($u' < 0, v' > 0$, Q2) and sweep ($u' > 0, v' < 0$, Q4) mo-

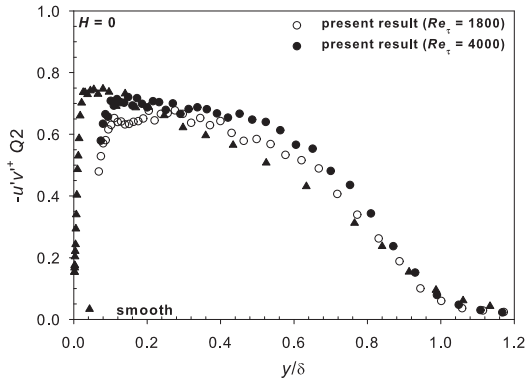

Figure 6. Wall-normal variation of Q2 events for H = 0.

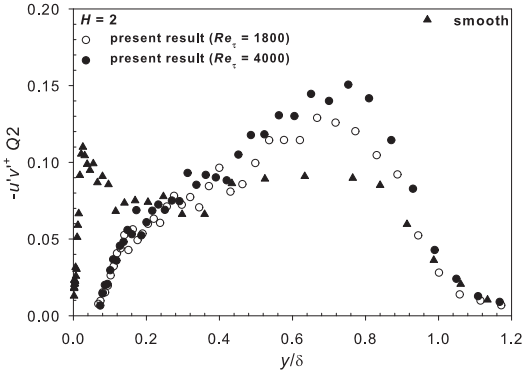

Figure 8. Wall-normal variation of Q2 events for H = 2.

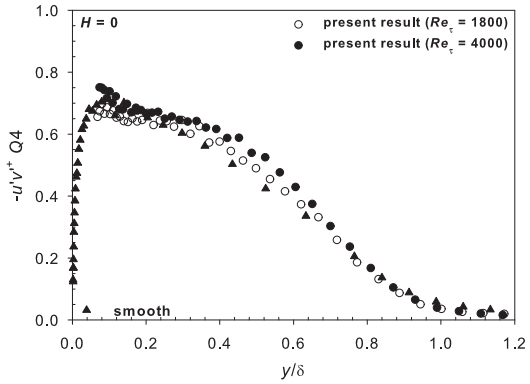

Figure 7. Wall-normal variation of Q4 events for H = 0.

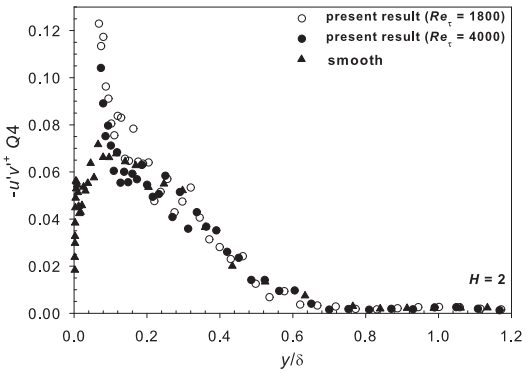

Figure 9. Wall-normal variation of Q4 events for H = 2.

tions to the total Reynolds shear stress to be calculated. The quadrant decomposition was carried out using the hyperbolic hole size (H) method of Lu & Willmarth (1973).

Figures 6 and 7 show the wall-normal variation of ejection (Q2) and sweep (Q4) contributions, respectively, to the Reynolds shears stress for H = 0. The figures that compare the two Reynolds numbers for the rough-wall case to the smooth-wall case indicate that all three cases have similar Q2 and Q4 contributions in the outer region. It can be seen that there is a marginal increase in the Q2 activity in the outer region for the sparse-roughness data. Schultz & Flack (2007) indicated that 3-D rough surfaces in the dense regime exhibit Q2 and Q4 contributions similar to that of smooth wall. This suggests that sparseness does not appear to affect Q2 and Q4 contributions from the overall Reynolds shear stress standpoint (i.e. for H = 0).

Figures 8 and 9 show the wall-normal variation of ejection (Q2) and sweep (Q4) contributions, respectively, to the Reynolds shear stress for H = 2. Using this threshold for H picks out strong fluctuation events where the Reynolds shear stress is larger in magnitude than $5\overline{u'v'}$. Figure 8 indicates that the ejection events in the outer region for the rough-wall case are much stronger compared to the smooth-wall case. However, the sweep events in the outer region for all three cases possesses similar strength. Schultz & Flack (2007) found that the Q2 and Q4 contributions (for H = 2) for rough-surfaces in the dense regime are similar to smooth-wall. The fact that Q2 events in the sparse regime are much stronger than the smooth-wall case suggests that the effect of sparseness is to increase the outward ejection of low-momentum fluid from the near-wall region. The increased Q2 activity contributes to the overall Reynolds shear stress which in turn results in increased drag. Moreover, these extreme ejection events are likely to play an important role in transport of scalars and pollutants, and its effect is likely to be felt throughout the boundary layer.

Planar measurements

The PIV measurements taken in the streamwise-spanwise plane can be utilised to explore the spatial structure of the turbulent boundary layers over sparsely distributed roughness elements. Figure 10 shows instantaneous contours of streamwise velocity fluctuation (u'^+, top figure) at Re_τ = 1800. The figure clearly reveals the presence of organisation in the form of forward-leaning structures of positive and negative fluctuations (or high- and low-momentum regions). Based on this instant, the inclination angle of the elongated region of high momentum in the center of figure (as marked with a black line) is found to be approximately 10°. Figure 10 also shows contours of wall-normal velocity fluctuation (v'^+,

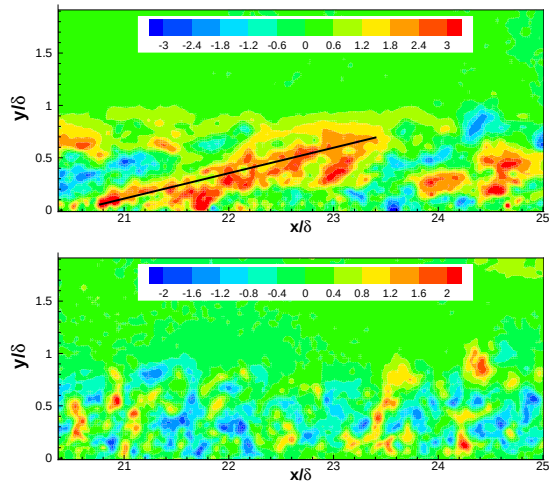

Figure 10. Instantaneous contours of u' (top) and v' (bottom) at Re_τ = 1800.

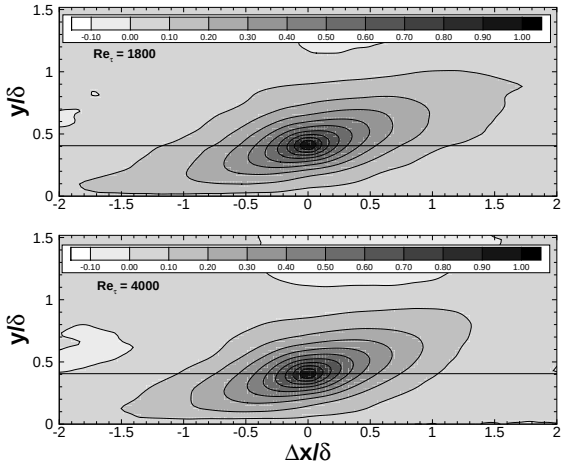

Figure 11. Two-point correlation of streamwise velocity fluctuations (R_{uu}). The top & bottom figures are for Re_τ = 1800 & 4000, respectively.

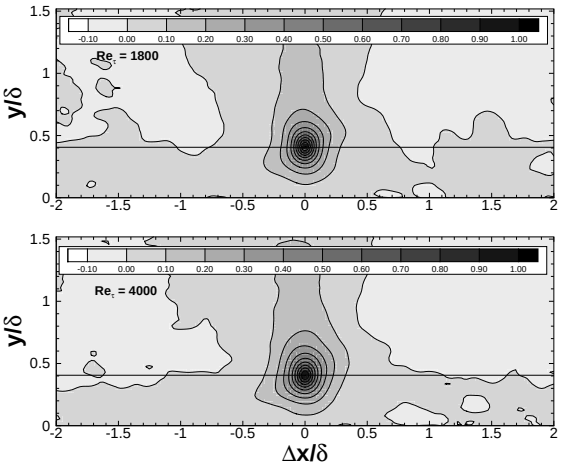

Figure 12. Two-point correlation of wall-normal velocity fluctuations (R_{vv}). The top & bottom figures are for Re_τ = 1800 & 4000, respectively.

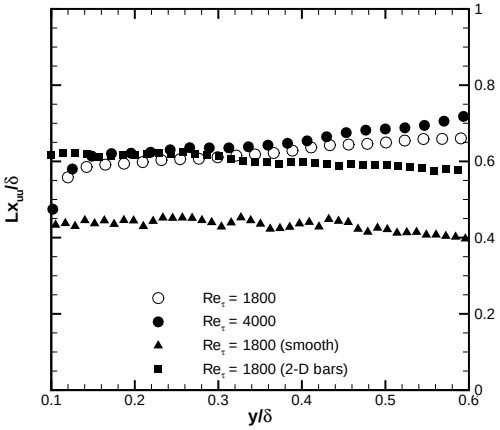

Figure 13. Wall-normal variation of streamwise length scale based on R_{uu} = 0.5 contour.

top figure) obtained at the same instant as u' (top figure). The figure shows that the wall-normal fluctuations are localised and do not exhibit any large-scale coherence. The coherence of both streamwise and wall-normal velocity fluctuations can be further explored by computing two-point correlations.

Figure 11 shows contours of the two-point correlations of the streamwise fluctuating velocity (R_{uu}) for both Reynolds numbers with the correlation centred at y_{ref}/δ = 0.4. The correlation structure at both Reynolds numbers indicates the presence of a forward-leaning structure that is consistent with the instantaneous contours in figure 10 and with findings in other rough- and smooth-surfaces. The inclination angle of the forward-leaning structure is approximately 13°, which is consistent with the inclination angle of the structure in flows over dense roughness as well as smooth walls. This indicates that the large-scale structure in smooth and rough-walls (of all types) have a similar organisation. There is very little difference between the two Reynolds numbers, however, this could be due to the lack of scale separation between the Reynolds numbers (with the higher Reynolds number just twice as high as the lower one). Figure 12 shows contours of the two-point correlations of the wall-normal fluctuations (R_{vv}) for both Reynolds numbers with the correlation centred at y_{ref}/δ = 0.4. The correlation structure at both Reynolds number indicates that the wall-normal fluctuations are spatially compact in both streamwise and wall-normal directions. This is consistent with the observations based on instantaneous fields and with the other rough- and smooth-wall flows (see Volino *et al.* (2009)).

The streamwise extent of the turbulence structure can be further explored by extracting R_{uu} along the streamwise direction in the reference plane as marked in figure 11. A stream-

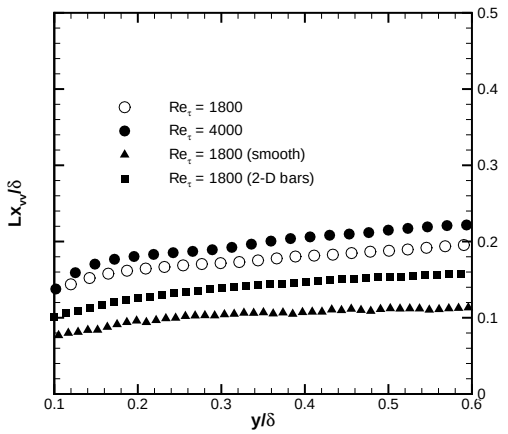

Figure 14. Wall-normal variation of streamwise length scale based on $R_{vv} = 0.5$ contour.

wise length scale is defined based on the cross-correlation (Lx_{uu}) as twice the distance from the self-correlation peak to the most downstream location on the $R_{uu} = 0.5$ contour. Figure 13 shows the wall-normal variation of the streamwise length scale (Lx_{uu}) based on R_{uu}. The figure shows that the length scales for the flow over sparse roughness elements are much higher than smooth and rough-wall cases. Streamwise extent of the coherence appear to be increased by 33-75% over the sparse roughness in the outer layer. The figure also shows the streamwise length scales for 2-D bar roughness (Volino *et al.* 2009). The 2-D case, which does not conform to outer-layer similarity, appears to follow the same trend as the sparse roughness near the wall. However, farther away from the wall ($y/\delta > 0.4$), the length scales for the sparse-roughness cases are larger than the 2-D bars case. It should be noted that λ_f for the 2-D bars is in fact in the region of transition between sparse and dense regime ($\lambda_f = 0.125$). It is not clear if the differences noted by Volino *et al.* (2007) and others in the 2-D bar case is due to two-dimensionality of the rough-surface or due to the fact that the 2-D bars are in the sparse regime.

Figure 14 shows the wall-normal variation of the streamwise length scale based on R_{vv} (using the same criteria as R_{uu}). The figure indicates that the streamwise extent of R_{vv} is increased by 75-90% over the sparse roughness when compared to smooth-wall or other rough-wall cases. The length scales for 2-D bars are larger than the smooth-wall case, however, it is smaller than the sparse-roughness case. This suggests that the increased intense Q2 activity occurs within structures that are larger than those found in flows over other surfaces. This aspect requires further investigation and will be an integral part of our future work.

Conclusions

Experiments were performed on a surface consisting of sparsely-distributed rigid circular cylinder roughness elements to examine the effects of solidity on turbulence structure. The solidity (λ) of the roughness (defined as frontal area of the roughness elements per unit wall-parallel area) is 0.08. Measurements were made using both two-component LDV and wide-field planar PIV techniques at two Reynolds numbers, Re_τ = 1800 and 4000. The results indicate mean velocity profile in defect form at both Reynolds numbers conforms to outer-layer similarity. The streamwise and wall-normal turbulence intensities exhibit reasonable similarity with smooth-wall results in the outer layer (i.e. for $y > 3k_s$), however, the Reynolds shear stress appear to be higher for the sparse roughness cases. The higher shear stress appears to be linked with strong ejection events that characterise the outer region of the flow. Moreover, the two-point spatial correlations of both streamwise and wall-normal velocity fluctuations computed using PIV data indicate that the turbulent structures in the outer region are coherent over much larger streamwise distances compared to smooth and other rough-wall cases. All these results point to the fact that sparseness plays an important role in the outer-layer structure of turbulent boundary layers over rough walls.

REFERENCES

AMIR, M. & CASTRO, I. P. 2011 Turbulence in rough-wall boundary layers: Universality issues. *Exp. Fluids.,* **doi: 10.1007/s00348-011-1049-7**.

FLACK, K. A., SCHULTZ, M. P. & CONNELLY, J. S. 2007 Examination of a critical roughness height for outer layer similarity. *Phys. Fluids* **19**, 095104.

JIMENEZ, J. 2004 Turbulent flows over rough walls. *Annu. Rev. Fluid Mech.* **36**, 173–196.

KROGSTAD, P. A. & ANTONIA, R. A. 1999 Surface roughness effects in turbulent boundary layers. *Exp. Fluids.,* **27**, 450–460.

LU, S. S. & WILLMARTH, W. W. 1973 Measurements of the structure of the Reynolds stress in a turbulent boundary layer. *J. Fluid Mech.* **60**, 481–511.

RAUPACH, M. R., ANTONIA, R. A. & RAJAGOPALAN, S. 1991 Rough-wall turbulent boundary layers. *Appl. Mech. Rev.* **4**.

SCHLICHTING, H. 1936 Experimentelle untersuchungen zum rauhigkeitsproblem. *Ing. Arch* **7**, 1–34, engl. transl. 1937. Experimental investigation of the problem of surface roughness. NACA TM 823.

SCHULTZ, M. P. & FLACK, K. A. 2007 The rough-wall turbulent boundary layer from the hydraulically smooth to the fully rough regime. *J. Fluid Mech.* **580**, 381–405.

VOLINO, R. J., SCHULTZ, M. P. & FLACK, K. A. 2007 Turbulence structure in rough- and smooth-wall boundary layers. *J. Fluid Mech.* **592**, 263–293.

VOLINO, R. J., SCHULTZ, M. P. & FLACK, K. A. 2009 Turbulence structure in a boundary layer with two-dimensional roughness. *J. Fluid Mech.* **635**, 75–101.

WALLACE, J. M., ECKELMANN, H. & BRODKEY, R. S. 1972 The wall region in turbulent shear flow. *J. Fluid Mech.* **54-1**, 39–48.